ACS OMEGA

http://pubs.acs.org/journal/acsodf

Article

Visible Light-Induced Reactive Yellow 145 Discoloration: Structural and Photocatalytic Studies of Graphene Quantum Dot-Incorporated TiO_2

Syeda Kinza Fatima, Ansumana Sangi Ceesay, Muhammad Saqib Khan,* Rizwana Sarwar, Muhammad Bilal, Jalal Uddin, Anwar Ul-Hamid, Ajmal Khan,* Nadia Riaz,* and Ahmed Al-Harrasi*

Cite This: *ACS Omega* 2023, 8, 3007−3016

Read Online

ACCESS | Metrics & More | Article Recommendations | Supporting Information

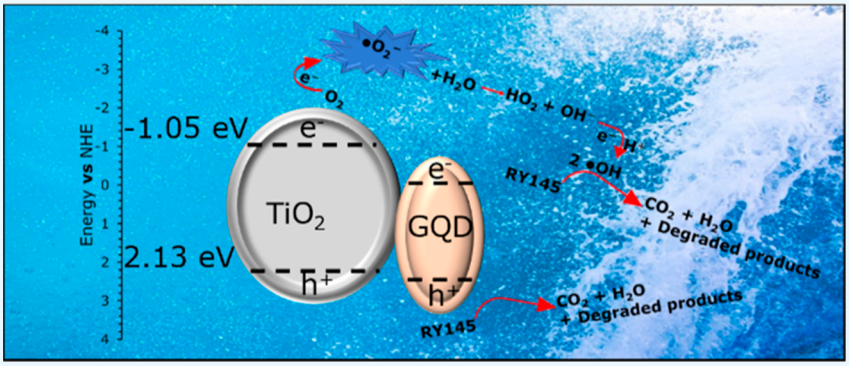

ABSTRACT: Visible light-induced photocatalytic treatment of organic waste is considered a green and efficient route. This study explored the structural and photocatalytic performance of graphene quantum dot (GQD)-incorporated TiO_2 nanocomposites to treat reactive yellow 145 (RY145) dye. For the effective removal of the RY145, efforts were made to better understand the kinetics of the process and optimization of the treatment parameters. Different GQD-doped TiO_2 nanocomposites were synthesized employing the sol−gel method. Physicochemical characteristics of the synthesized nanocomposites were studied through FTIR, XRD, UV−visible spectroscopy, SEM, and EDX. Screening studies were conducted for synthesis and reaction optimization. The results indicated that GQD−TiO_2 significantly enhanced the photocatalytic discoloration for RY145 dye. Among the synthesized nanocomposites, 15GQD−TiO_2 calcined at 300 exhibited 99.3% RY145 discoloration in 30 min under visible light irradiation. Following the pseudo-first-order reaction, the photocatalytic reaction constant K_{app} progressively declined with an increase in the concentration of RY145. The heterogeneous reaction system conformed to the Langmuir−Hinshelwood isotherm, as indicated by the K_C (1.08 mg L^{-1} min^{-1}) and the K_{LH} (0.18 L mg^{-1}) values. $O_2^{\bullet-}$ was found to be the major contributor in GQD−TiO_2-300 to decolorize RY154, while TiO_2 and GQDs played a vital role in generation of electrons and holes. Additionally, after recycling to the seventh cycle, only 9% decline in photocatalytic performance was observed for the synthesized nanocomposite.

1. INTRODUCTION

With the rapid increase in industrialization, urbanization, and economic development, environmental pollution is becoming a more serious problem for the human society. Discharge of synthetic toxic pollutants such as dyes, pesticides, pharmaceuticals, and so forth, due to these anthropogenic activities, in water is increasing and endangering humans and the entire biosphere. As a result, it is vital to figure out a solution to the major cause of water pollution control and purification. Organic dyes are among the main contaminants released as industrial effluents into waterways. Dyes are used as colorants in the manufacturing of textiles, cosmetics, foods, pharmaceuticals, materials, paintings, pigments, prints, and papers.[1] The most popular and widely used synthetic dyes are azo dyes,[2] which consist of a distinctive double bond between the two nitrogen atoms in their chemical structure (−N═N−) with other group associations such as sulfonic groups. These bonds are not easily biodegradable, and the recalcitrant nature of the dye is retained. Textile dyeing effluents contain 5−50% of reactive dyes (azo dyes).[3] Various reports showed that textile effluents have detrimental effects on the growth rate of vegetation which are ecologically important.[4] Hence, water purification is necessary for the textile effluents. Many

Received: September 7, 2022
Accepted: November 14, 2022
Published: January 10, 2023

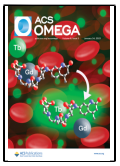

traditional treatment processes are being used such as biological,[5] adsorption,[6] oxidation,[7] extraction,[8] coagulation, flocculation,[9] and so forth; however, these conventional methods are no longer successful due to advancements in coloring technology and the complex dye structure. Therefore, it is imperative to develop a treatment process that not only eliminates these resistant textile pollutants but also enhances water quality.

Graphene quantum dots (GQDs) have been recently being focused on the field of nanotechnology for the environmental remediation approaches because of their high stability, anomalous physicochemical properties, and unique photoluminescence properties.[10] GQDs have also been investigated as a possible replacement of TiO_2 (a widely used photocatalyst).[11] TiO_2 has significant popularity for eliminating dyes from wastewater due to their larger surface area, adsorption capacity, and faster equilibrium rates. However, due to the wide band gap, TiO_2 can only participate in photocatalytic action when presented to UV light that comprises only 4% of the visible region.[12]

However, to fully utilize the remediation properties of TiO_2, the alteration of TiO_2 is necessary to improve the photocatalytic capabilities. A significant number of studies on TiO_2 alteration to improve its photocatalytic capabilities have been reported. These modifications include doping (metal/nonmetal),[13] surface modification,[14] dye sensitization,[15] composite synthesis with a variety of different materials,[16] and immobilization and stabilization on support structures.[17] Recent studies have reported that due to their high catalytic activity and almost 100% atom consumption, metal-based atomically dispersed catalysts have gained increased attention.[18] However, very little focus is given to the possible potential of GQD−TiO_2 combination. GQDs have been reported as a sensitizer for semiconductor catalytic materials, and they significantly improve the catalytic performance of these materials[19] through absorption of visible light.

The photocatalytic process of TiO_2 and GQD−TiO_2 is the same; however, the difference lies in the improvement of the efficiency. When exposed to visible light, GQDs photosensitize TiO_2 and contribute electrons to its conduction band. This improves the TiO_2−GQD nanocomposites' capacity to absorb visible light.[20] Chinnusamy et al. attributed the higher photocatalytic activity of GQD−TiO_2 to the efficient charge separation at the interface of GQD−TiO_2.[21] Mechanistic studies showed that the large energy difference between the LUMO of the GQDs above the conduction band (CB) of TiO_2 drives the electron transfer from the CB of the GQDs to the CB of TiO_2.[22] Moreover, GQDs can serve as an electron sink for photogenerated electrons due to their unique electronic properties and high electronic conductivity, thus facilitating electron donor−acceptor interaction between GQDs and TiO_2.[23] It is clear from the literature that doping GQDs with photocatalytic improves their photocatalytic capacity and shifts the reaction into the visible light range.

2. MATERIALS AND METHODS

All the chemicals utilized in this study were of analytical grade and used without further refinement. The commercial-grade reactive yellow 145 (RY145) were provided by Koh-i-noor textile industry (Pakistan), and titanium tetraisopropoxide (TIP), 98% purity, was purchased from Dae-Jung Chemicals (South Korea), while citric acid (CA) and absolute ethanol (98%) were obtained from Merck (Germany).

2.1. Synthesis of GQDs and GQD−TiO_2 Nanocomposites. Citric acid was pyrolyzed to obtain GQDs, as described previously.[24] In a typical procedure, a desired amount of citric acid was heated on isomantle for 5 min at 200 °C. Initially, CA was liquidated to colorless liquid, and after 5 min, the color changed to orange. The resultant orange liquid was neutralized with ethanol containing 10 mg L^{-1} NaOH. After neutralization, the color changed to pale yellow, indicating GQD formation.[24,25]

GQD incorporation @TiO_2 was achieved through the modified sol−gel method described in our previous study.[26] 37 mL TiO_2 precursor, TIP was poured into 60 mL of ethanol. In another solution 15 mL acetic acid, 20 mL absolute ethanol and desired amount GQDs and 10 mL DI distilled water was added. The GQD solution was gradually introduced to TiO_2 precursor solution under vigorous stirring. The obtained gel was aged overnight under ambient conditions (22 °C ± 1). Afterward, the gel was dried in an oven at 90 °C for 24 h. The dried powder was ground into powder and annealed for 60 min at various calcination temperatures, that is, 300, 400, and 500 °C. The list of the synthesized nanocomposite is depicted in the first column of Table 1.

Table 1. XRD Crystallite Size of Different Synthesized Nanocomposites

nanocomposite	FWHM (rad)	crystallite size (nm)	band gap energy (eV)
1GQD−TiO_2-300	0.024	5.84	3.01
1GQD−TiO_2-400	0.024	5.87	3.03
1GQD−TiO_2-500	0.013	10.58	3.12
15GQD−TiO_2-300	0.025	5.48	2.91
15GQD−TiO_2-400	0.023	5.99	3.18
15GQD−TiO_2-500	0.012	11.72	3.16

2.2. Evaluation of Photocatalytic Performance. Photocatalytic discoloration studies were performed using the synthesized nanocomposite, according to the protocol described in ref 27. All the experiments were performed under ambient conditions, temperature (21 ± 1 °C), nanocomposite dosage (1 mg mL^{-1}), and RY145 concentration (30 mg mL^{-1}); Prior to the addition of RY145 dye, the synthesized nanocomposite was sonicated in DI distilled water. Afterward, adsorption desorption equilibrium was achieved for 10 min before the exposure to visible light (wavelength: 400−700 nm and intensity: 30,798 lux). Aliquots were sampled at predefined intervals during the irradiation experiment to measure the change in dye concentration, and each aliquot was centrifuged and analyzed through a UV−vis spectrophotometer (PG Instruments Ltd., UK) at 419 nm. The following equation (eq 1) was used to calculate the RY145 discoloration performance (%).

$$\%\ \text{RY145 decolorization} = \left(\frac{C_o - C_t}{C_o}\right) \times 100 \quad (1)$$

where C_o is the RY145 initial concentration (mg L^{-1}) and C_t is the RY145 concentration at time (mg mL^{-1}).

The effect of different reaction parameters such as reaction pH, nanocomposite dose, and RY145 concentration was also checked on the performance of the best screened nanocomposite.

https://doi.org/10.1021/acsomega.2c05805
ACS Omega 2023, 8, 3007−3016

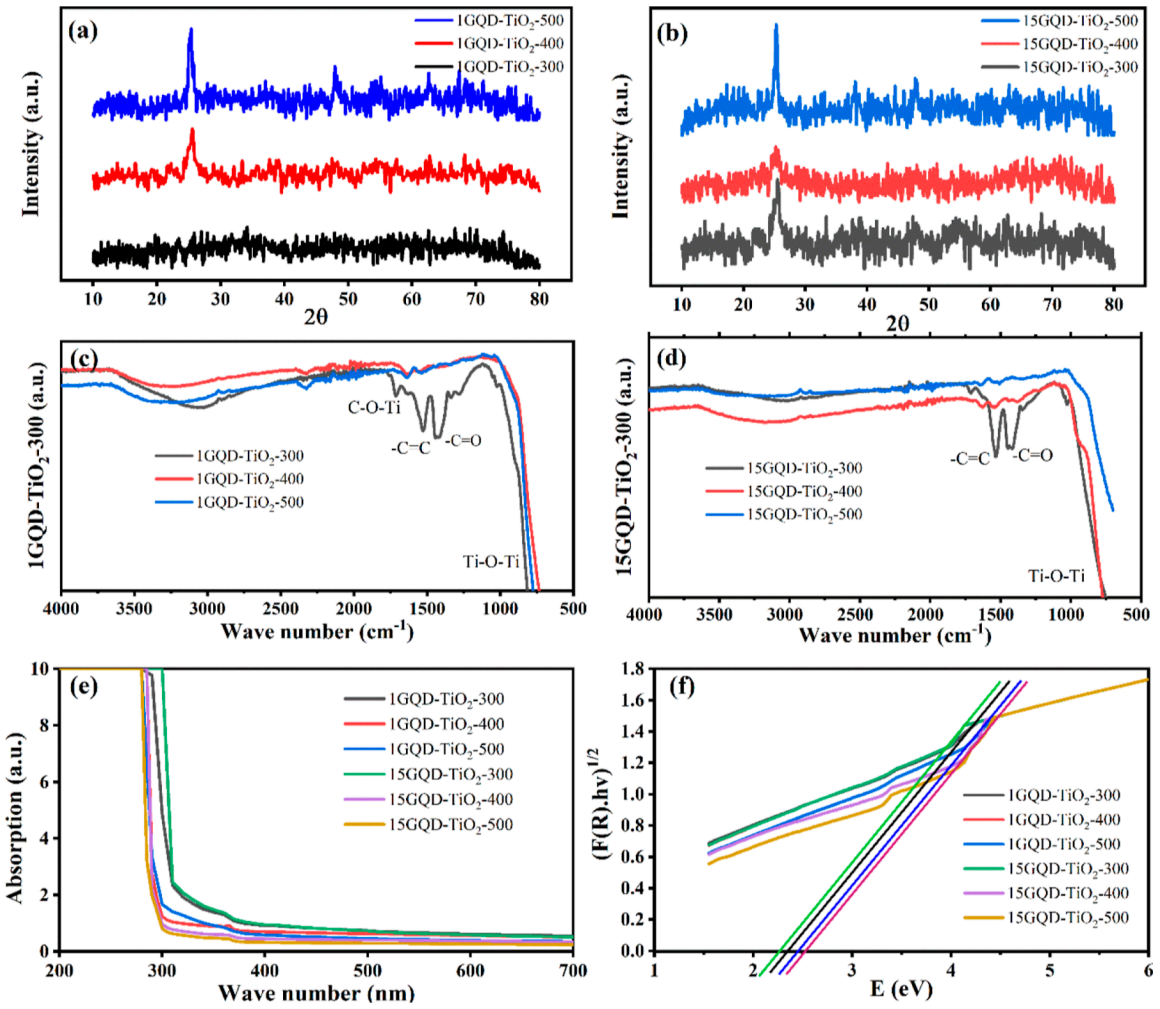

Figure 1. Physicochemical properties of the synthesized nanocomposite: XRD analysis: (a) 1GQD−TiO_2 and (b) 15GQD−TiO_2; FTIR analysis: (c) 1GQD−TiO_2 and (d) 15GQD−TiO_2; and UV−visible analysis: (e) absorption spectrum and (f) band gap estimation.

2.3. Photocatalytic Kinetics. Photocatalytic discoloration rate was explored by fitting the experimental data into the Langmuir−Hinshelwood (LH) model[28] using the following LH expression

$$\frac{1}{r_o} = \frac{1}{K_C} + \frac{1}{K_C K_{LH}} \times \frac{1}{[RY145]_e} \quad (2)$$

Equation 2 corresponds to the relation of $1/r_o$ and $[RY145]_e$ concentration values. Moreover, K_c and K_{LH} demonstrate the effect of RY145 concentration on the equilibrium constant.

2.4. Characterization of the Synthesized Nanocomposite. The physicochemical properties of the synthesized nanocomposite were studied using different characterization techniques; these included Fourier transform infrared spectroscopy (FTIR; Alpha Bruker, Karlsruhe, Germany), X-ray diffraction (XRD; Bruker, Billerica, Massachusetts, United States), UV−visible spectroscopy (T80$^+$ series PG Instruments Ltd., UK), scanning electron microscopy (SEM), and energy-dispersive X-ray spectroscopy (EDS) (JEOL JSM-6510LA, Tokyo, Japan).

2.5. Active Species Trapping Experiments. To understand the mechanism and role of various active species in the photocatalytic reaction, scavenging or active species trapping studies were carried out as described previously.[25] Before the addition of the nanocomposite, various scavengers were used in the reaction solution of RY145; these included isopropyl alcohol (IPA), benzoquinone, and disodium ethylenediaminetetraacetate (EDTA) as scavenging agents for $^{\bullet}OH$, $O_2^{\bullet-}$, and h^+, respectively.

2.6. Durability Studies. Durability of the nanocomposite was checked through recycling. Studies were conducted to check the recycling potential of the synthesized nanocomposite. The photocatalytic reaction was carried out in eight cycles, and after each cycle, 15GQD−TiO_2-300 was retrieved from the reaction solution through centrifugation followed by washing and drying. All the experimental conditions were kept the same for each experiment. The discoloration (%) was determined using eq 1.

3. RESULTS AND DISCUSSION

3.1. Diffraction Analysis (XRD). The XRD patterns of 1GQD−TiO_2 and 15GQD−TiO_2 calcined at 300, 400, and 500 °C are depicted in Figure 1a−c. The characteristic diffraction peaks that appeared at 25.33, 33.65, 47.45, 54.59, and 76.81° are attributed to (1 0 1), (0 0 4), (2 0 1), (2 1 1), and (1 8 4) planes of anatase TiO_2 (JCPDS # 21-1272). In addition, similar peaks were observed for all the GQD-incorporated TiO_2, and no phase transformation was observed even at higher calcination temperature (500 °C). These results demonstrate the inhibition of TiO_2 phase change by GQD

https://doi.org/10.1021/acsomega.2c05805
ACS Omega 2023, 8, 3007−3016

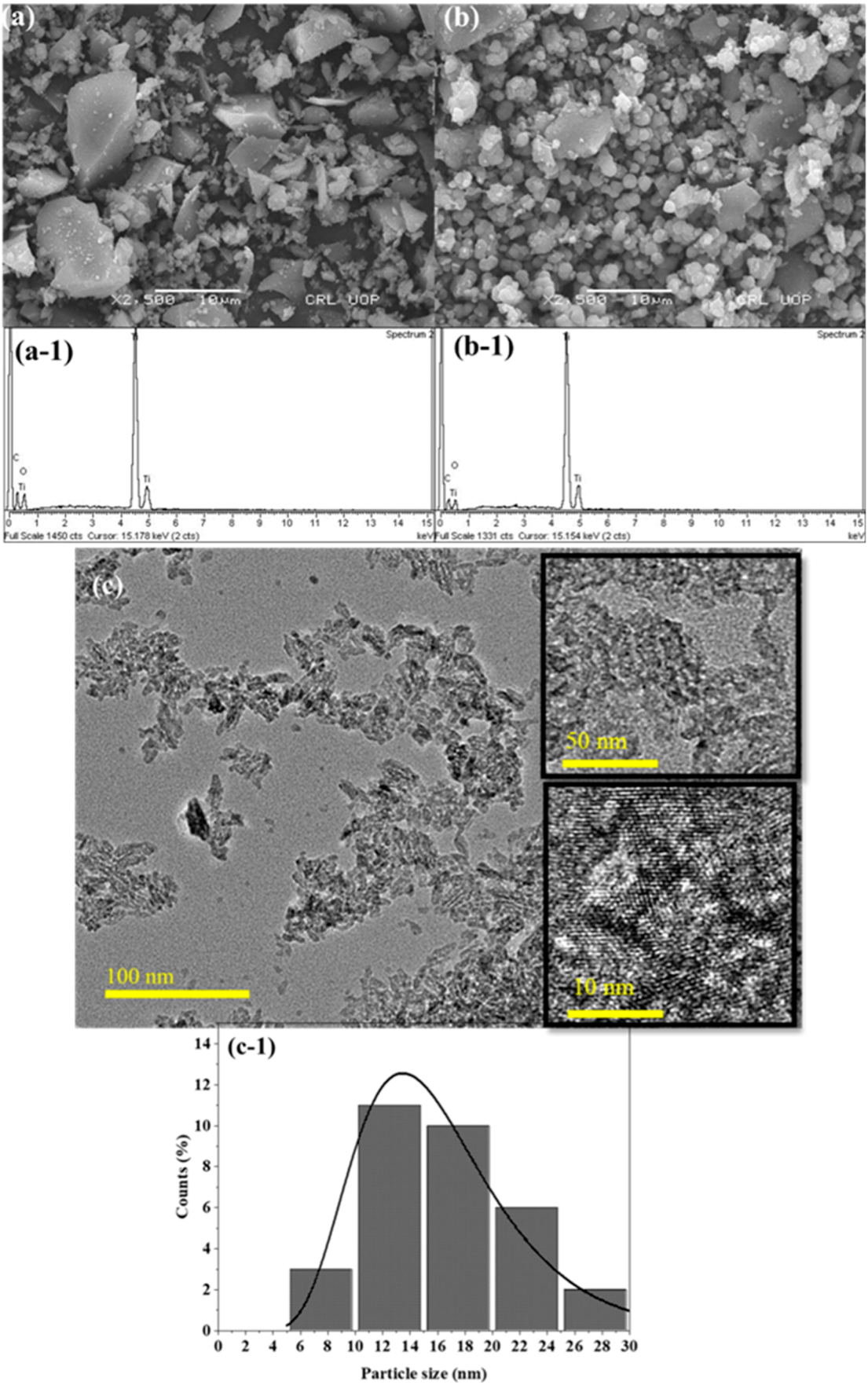

Figure 2. SEM images of (a) 1GQD−TiO_2-300 and (b) 15GQD−TiO_2-300 and EDX spectrum of [a(1)] 1GQD−TiO_2-300 and [b(1)] 15GQD−TiO_2-300, (c) TEM images of 15GQD−TiO_2-300 and [c(1)] TEM particle size distribution.

https://doi.org/10.1021/acsomega.2c05805
ACS Omega 2023, 8, 3007−3016

introduction. This inhibition of the phase transformation may be caused by the Ti−O−C bond, which is thought to prevent the transformation of the anatase octahedral spiral chain into the rutile octahedral straight chain;[29] the results of FTIR are also in the favor of XRD findings. In addition, there is no new diffraction peak in GQD−TiO_2, indicating that GQDs were successfully decorated on the TiO_2 surface without altering the crystalline structure of TiO_2. No diffraction peak of carbon (GQD) was recorded in the XRD pattern which can be due to the high dispersion and low concentration of carbon contents in TiO_2; however, the carbon content presence were detected in the EDS mapping and FTIR analysis of these samples.[25] Table 1 shows the comparison of crystallite size of different synthesized nanocomposites.

3.2. Functional Group Analysis (FTIR). FTIR analysis was also performed to further understand the physicochemical properties of the nanocomposites and effect of different synthesis parameters. Figure 1c,d shows the FTIR spectra of 1GQD−TiO_2 and 15GQD−TiO_2 calcined at 300, 400, and 500 °C. The O−C−O asymmetric and symmetric vibrations were recorded at ∼1593 and ∼1416 cm^{-1}, respectively, while the C═O group existed at ∼1090 and ∼990 cm^{-1}, and the C−O−Ti peak was around 2131 cm^{-1}.[30] The stretching vibrations of Ti−O−Ti were observed around the 400−900 cm^{-1} range.[31,32] Moreover, the increase in annealing temperature from 300 to 500 °C reduced the intensity of the corresponding absorption peaks.

3.3. Band Gap Analysis. UV−visible spectroscopy was employed to estimate the band gap of the synthesized nanocomposites. Figure 1e depicts the absorption spectrum of the synthesized nanocomposites, and corresponding band gap energies are given in Figure 1f. Absorption of visible light was recorded for 1GQD−TiO_2-300 and 15GQD−TiO_2-300 compared to other GQD loadings and calcination temperatures. Previous studies demonstrated that the excitation of electrons from the valence band (VB) to the conduction band (CB) is caused by the sharp absorption edge at 390 nm.[33] The band gap was estimated through Tauc's plot by plotting $(F(R)\ h\nu)^{1/2}$ versus band gap energy. The band gap of TiO_2 is 3.19 eV, while the band gap calculated for GQDs used in this study was 2.20 eV (Figure S1, Supporting Information). The results depicted reduction in the TiO_2 band gap of 2.91 eV after decoration of 15GQD−TiO_2-300. Our results are consistent with previous studies which show reduction in band gap upon the introduction of metals or nonmetal moieties into the lattice structure of TiO_2.[25,32]

3.4. Surface Morphology Analysis (SEM). Figure 2a,b, depicts the morphological characteristics of the best performing nanocomposite calcined at 300 °C, that is, 1GQD−TiO_2 and 15GQD−TiO_2, and the corresponding EDS analysis is shown in Figure 2a(1),b(1). In both nanocomposites, dispersed particles were observed; however, there is a noticeable variation in the crystallinity. These results agree with the XRD findings, where clear anatase peaks were observed for 15GQD−TiO_2-300, while no such crystalline peaks were observed for 1GQD−TiO_2-300. The major chemical components obtained through EDS element mapping were Ti, C, and O over the entire region. According to these findings, coating-like heterojunctions are formed between GQDs and TiO_2 with a firm and close contact.[22] The synthesized GQD/TiO_2 nanocomposites analyzed using TEM [as in Figure 2c(1)] indicated spherical agglomerated morphology, with an average particle size of ∼2.73 ± 0.35 nm and dispersion in the form of sheet.

3.5. Screening and Optimization Studies. *3.5.1. Effect of Calcination Temperature and GQD Loading.* Reaction studies were conducted for the selection of the best combination of calcination temperature and GQD loading. The discoloration efficiency (%) for each nanocomposite is depicted in Table 2. The results revealed that the best combination was 15 mol % GQD loading and 300 °C calcination temperature with a discoloration efficiency of 99.8% in 30 min of reaction. Any increase in calcination temperature and GQD loading resulted in reduced photocatalytic efficiency. The higher calcination temperature might result in the loss of carbon (GQD) contents, which are visible in the FTIR analysis, showing less intense IR peaks upon calcination. Moreover, at higher GQD loading, the surface contact between TiO_2 and RY145 can decrease due to which less production of free radicals and charge carrier dissipation by trapping above a certain level of GQD loading occur.[34] In addition, the photons are obscured by GQDs, preventing the charge transfer and OH radical production,[22] ultimately reducing the photocatalytic efficiency. Furthermore, higher GQD content in the composite results in GQD aggregation, which inhibits the GQD and TiO_2 interaction, resulting in lower photocatalytic activity.[21]

Table 2. Effect of Calcination Temperature and QD Loading on Discoloration of RY145

	discoloration (min^{-1})		
GQD loading (mol %)	300 °C	400 °C	500 °C
TiO_2	5.50×10^{-3}	5.20×10^{-3}	7.10×10^{-3}
1GQD−TiO_2	1.38×10^{-1}	1.97×10^{-2}	1.43×10^{-2}
5GQD−TiO_2	1.26×10^{-1}	1.77×10^{-2}	1.43×10^{-2}
10GQD−TiO_2	1.38×10^{-1}	1.68×10^{-2}	1.44×10^{-2}
15GQD−TiO_2	1.54×10^{-1}	1.18×10^{-2}	1.61×10^{-2}
20GQD−TiO_2	3.00×10^{-2}	2.71×10^{-2}	1.96×10^{-2}
30GQD−TiO_2	2.31×10^{-2}	1.63×10^{-2}	1.56×10^{-2}

3.5.2. Effect of Irradiation Time. Figure 3a depicts the effect of irradiation time on the discoloration efficiency of the 15GQD−TiO_2-300 nanocomposite. The reaction was conducted for 60 min; however, 99.8% RY145 discoloration was achieved in first 30 min of visible light irradiation. In our previous study, the reaction time was 60 min with different metals (Fe, Cu, and Ni) for the degradation of RY145;[27] however, GQD introduction into the TiO_2 reduced the reaction time to 30 min. This can be attributed to better e^-/h^+ transfer at the optimum GQD loading and generation of OH radicals. Based on these results, the irradiation time was set for 30 min in the rest of the study.

3.5.3. Effect of Nanocomposite Dose. The effects of nanocomposite dose on RY145 discoloration efficiency of 15GQD−TiO_2-300 are depicted in Figure 3b. The nanocomposite dose was varied from 0.25 to 2.0 mg L^{-1} for a reaction volume of 60 mL. The discoloration efficiency for 15GQD−TiO_2-300 was initially decreased with increasing nanocomposite dose; maximum efficiency was observed when the nanocomposite dose reached 1 mg mL^{-1}. However, as the nanocomposite dose increased, the discoloration efficiency decreased. These results are contrary to the usual observation that increasing the active sites through increasing the nanocomposite contents should increase nanocomposite

https://doi.org/10.1021/acsomega.2c05805
ACS Omega 2023, 8, 3007−3016

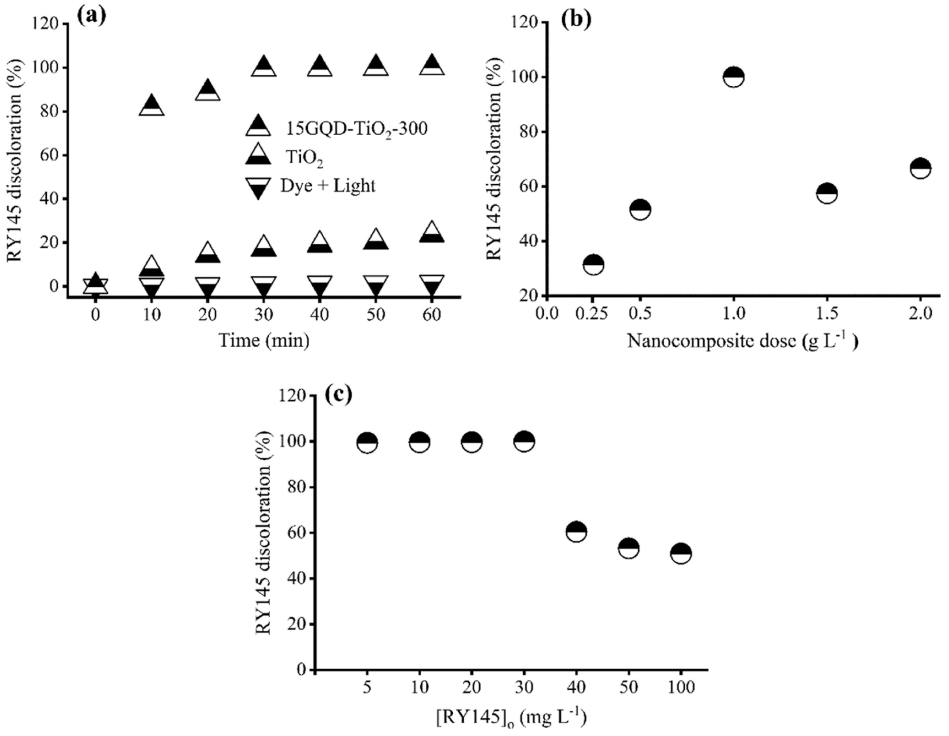

Figure 3. Effect of different reaction parameters on discoloration of RY145: (a) reaction time, (b) nanocomposite dosage, and (c) initial RY145 dye concentration.

efficiency, however, as a heterogeneous photocatalytic reaction depends on the availability of photons, and increasing the nanocomposite dose causes the reaction solution to become turbid, which prevents the photons from reaching the nanocomposite surface and reduces the efficiency of the nanocomposite. Similar findings are reported in previous heterogeneous photocatalytic studies.[35−37] The rest of the study was conducted using an optimum dose of 1 mg mL^{-1}.

3.5.4. Effect of Initial Dye Concentration. The effect of initial dye concentration was investigated for 5, 10, 20, 30, 40, 50, 60, and 100 mg L^{-1} of the RY145 (Figure 3c). During the experiment, the initial dye concentration was varied, while other reaction conditions such as an ambient temperature of 21 ± 1 °C, 1 mg L^{-1} nanocomposite dose, and working pH were kept constant. Higher discoloration efficiency was achieved at lower initial RY145 concentrations, but after reaching an optimal concentration level (40 mg L^{-1}), the nanocomposite efficiency significantly reduced, and at higher dye concentrations, the RY145 reaction solution becomes blurry and photons cannot reach the nanocomposite surface, and very few free radicals are produced, which in turn lowers the efficiency.

3.6. Adsorption Studies. Studies were conducted to assess the adsorption behavior of the synthesized nanocomposite. Results depicted in Figure 4 revealed that the nanocomposite decorated with GQDs had higher adsorption capacity compared to TiO_2. TiO_2-300, TiO_2-400, and TiO_2-500 showed adsorption capacities of 0.0503, 0.0587, and 0.0372 mg g^{-1}, respectively, compared to GQD−TiO_2 nanocomposites. 15GQD−TiO_2-300 and 1GQD−TiO_2-300 demonstrated maximal adsorption capacities of 0.1218 and 0.1142 mg g^{-1}, respectively, in 60 min of batch reaction. In addition, it was found that adsorption capacity decreased with the increase in calcination temperature. Previous research

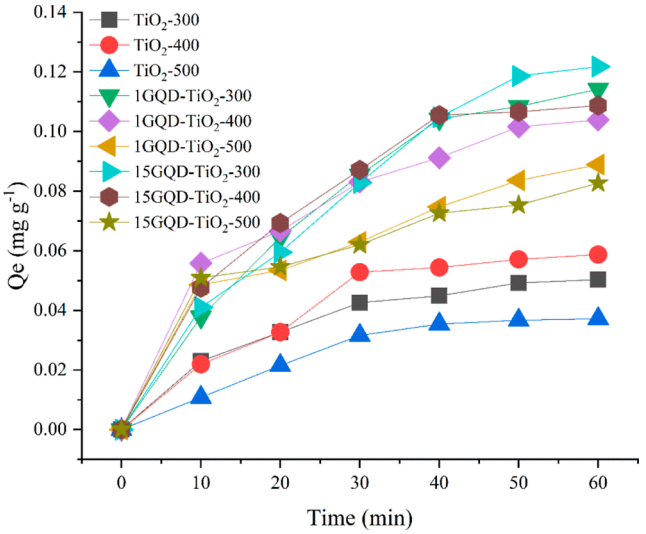

Figure 4. Adsorption studies of the synthesized nanocomposites.

demonstrated that the decoration of graphene on TiO_2 increases the pore size and surface area, which ultimately increase the adsorption capacity[38,39]

3.7. Kinetic Studies. Kinetic studies are important in terms of understanding the reaction and reaction rate. The discoloration data obtained at different concentrations using the 15GQD−TiO_2-300 nanocomposite were fitted into different kinetic models including first-order (FO), pseudo-first-order (PFO), zero-order (ZO), and second-order (SO) models for quantitative assessment. The best fit model was selected based on R^2. The PFO kinetic model is presented in Figure 5, while the other kinetic models are presented in Figure S2a−c. The rate constant (K) for different kinetic models is depicted in Table 3. The photocatalytic discoloration

https://doi.org/10.1021/acsomega.2c05805
ACS Omega 2023, 8, 3007−3016

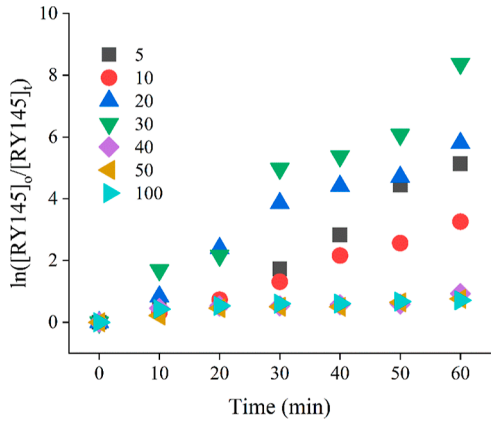

Figure 5. PFO reaction kinetics for the discoloration of RY145 using 15GQD−TiO_2-300.

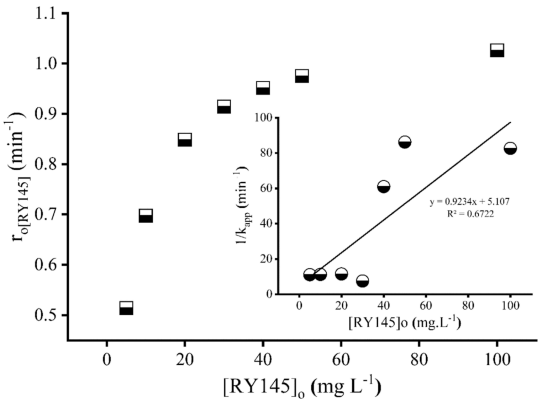

Figure 6. Effect of RY145 initial concentration on the discoloration rate using 15GQD−TiO_2-300, inset $1/K_{app}$ of discoloration against initial dye concentration.

reaction of RY145 using 15GQD−TiO_2-300 fits to PFO reaction kinetics.

3.7.1. Heterogeneous Photocatalytic Isotherm Studies. The photocatalytic reaction mechanism of the discoloration of RY145 dye through 15GQD−TiO_2-300 was studied using the Langmuir−Hinshelwood (LH) isotherm. The reaction rate (min^{-1}) was determined for each concentration and is depicted in Figure 6. The results showed that the effectiveness of the 15GQD−TiO_2-300 nanocomposite for RY145 dye discoloration decreased as dye concentration increased. Moreover, a significant effect was observed on the reaction rate with increasing dye concentration, and lower RY145 dye concentrations showed a faster reaction rate, while higher concentrations showed a slower reaction rate. The slower reaction rate can be explained by the fact that at higher concentrations, more RY145 molecules are adsorbed on the surface of the 15GQD−TiO_2-300 nanocomposite and fewer photons reach the nanocomposite's surface, which ultimately reduces the nanocomposite's photocatalytic efficiency. Similar findings are reported in refs 40−4142. The Figure 6 inset shows the LH expression by plotting the reciprocal of apparent rate constant against initial RY145 concentration. The K_{LH} value obtained was 0.18 L mg^{-1}, while K_C was 1.08 mg L^{-1} min^{-1}. Furthermore, theoretical evaluation of the photo discoloration of RY145 can be obtained by applying the value obtained from the LH model to eq 3

$$\frac{1}{r_o} = \frac{0.195}{[RY145]_O} + 0.923 \quad (3)$$

3.8. Recycling Studies. Stability and durability studies are important from an economic point of view, as it determines the widespread concern related to future application of the as-synthesized nanocomposite. In this regard, the recycling potential was measured with multiple cycles to assess 15GQD−TiO_2-300 nanocomposite reusability. After each reaction cycle, the utilized nanocomposite was recovered by centrifugation followed by washing and drying. The results depicted in Figure 7 show multiple cycles of RY145

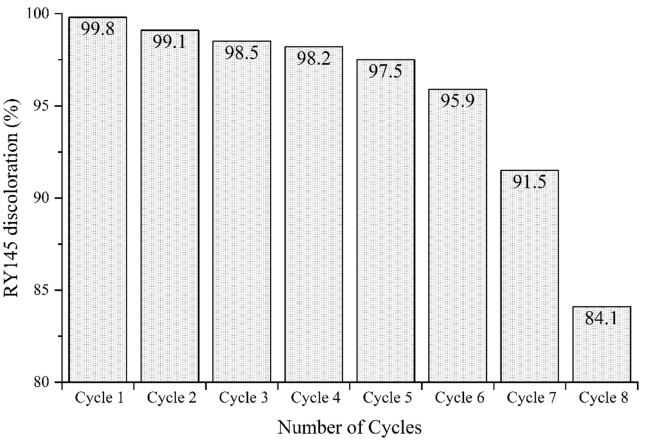

Figure 7. Recycling studies of the best performing nanocomposite (15GQD−TiO_2-300).

discoloration. The as-synthesized 15GQD−TiO_2-300 nanocomposite showed only lost 9% in RY145 discoloration efficiency and was durable until the seventh cycle, and a slight decline of 7% was observed in the eighth cycle (84% discoloration). These results indicate that the GQD addition to the TiO_2 is much stable compared to other metal/nonmetal dopants.[25,43]

3.9. Photocatalytic Mechanism Studies. As photocatalytic reaction is governed by reactive species including $^{\bullet}OH$, $-O_2$, e^-, and h^+, to determine their role in the reaction, scavenging or trapping experiments were conducted using

Table 3. Rate Constants of Different Kinetic Models Using the 15GQD−TiO_2-300 Nanocomposite

concentration (mg L^{-1})	PFO (mg L^{-1} min^{-1})	ZO (mg L^{-1} min^{-1})	FO (mg L^{-1} min^{-1})	SO (mg L^{-1} min^{-1})
10	0.0808	0.0281	−0.0808	11.083
20	0.097	0.0463	−0.097	13.787
30	0.1325	0.0109	−0.1325	115.89
40	0.0111	0.0177	−0.0111	0.0338
50	0.0113	0.0317	−0.0113	0.0281
100	0.0097	0.044	−0.0097	0.0097

https://doi.org/10.1021/acsomega.2c05805
ACS Omega 2023, 8, 3007−3016

different scavenging agents, as discussed earlier in Section 2.5. The photocatalytic performance of 15GQD−TiO_2-300 was markedly reduced to 87% in the presence of BQ which indicated strong participation of superoxide radicals ($O_2^{\bullet-}$) or the photogenerated electrons. Moreover, 71 and 51% reduction were observed in the presence of EDTA (h^+) and IPA ($^\bullet$OH), respectively (Figure 8). These findings indicate that although all reactive species were involved in the photocatalytic reaction, however, superoxide played a vital role in discoloration of RY145 dye.

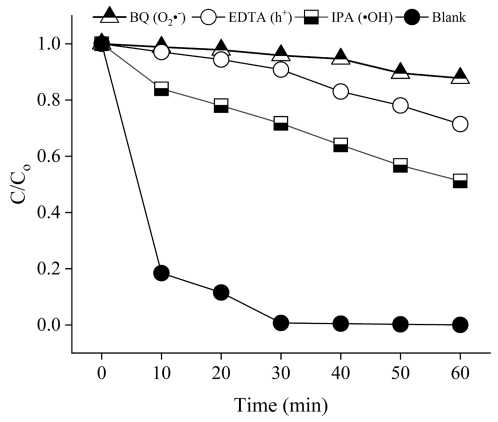

Figure 8. Effect of different scavenging agents on the photocatalytic performance of 15GQD−TiO_2-300.

The photocatalytic mechanism is further confirmed through determining the energy positions of the conduction band (CB) and valence band (VB). The Mulliken electronegativity and corresponding band gap value were used to derive the nanocomposite's CB and VB positions using the following equation.

$$E_{CB} = \chi - E^e - 0.5E_g \quad (4)$$

$$E_{VB} = E_{CB} - E_g \quad (5)$$

E_{CB} and E_{VB} are the band gap CB and VB potential of the conduction and valence band, respectively, E^e is the energy of free electron versus hydrogen, and χ is the geometric mean of the Mulliken electronegativity constituent.[44] χ was calculated as

$$\chi = [x(A)^a \cdot x(B)^b \cdot x(C)^c]^{1/a+b+c} \quad (6)$$

where a, b, and c are the number of atoms in the compound. The CB_{TiO2} and CB_{GQDs} were −1.05 and 0.36 eV, respectively, while VB_{TiO2} and VB_{GQDs} were 2.13 and 3.16 eV versus normal hydrogen energy (NHE), respectively. The band positions are shown in Figure 9. In visible light irradiation, the energy of the excited photon can super pass the energy gap of GQDs and TiO_2 to produce e^- and h^+ pairs. As the CB and VB of TiO_2 are higher than the CB and VB of GQDs, the electrons generated in GQDs shall pass on to the CB and VB of TiO_2. Since the CB_{TiO2} is more negative, the photoexcited electron on the CB of TiO_2 (−1.05 eV) will react with H_2O ($E_{H_2O}/^\bullet$OH = 2.38 eV) or OH^- ($E_{OH^-}/^\bullet$OH = 1.99 eV) to produce hydroxyl radicals ($^\bullet$OH) (2.38 V) and superoxide anion radicals ($O_2^{\bullet-}$) ($EO_2/O_2^{\bullet-}$ = −0.33 eV). The proposed mechanism is supported by the scavenging experiments and the strong role of $O_2^{\bullet-}$ in the discoloration of RY145.

CONCLUSIONS

This study reports the textile wastewater purification through a green and efficient route of the advance oxidation process using GQD-anchored titanium dioxide at the lab-scale photocatalytic reactor under visible light. Different-weight-percent-GQD-embedded TiO_2 nanocomposites were synthesized via pyrolysis and the sol−gel method. The structural and photocatalytic performance of the synthesized nanocomposites against RY145 dye discoloration was studied using UV−visible spectroscopy, FTIR, XRD, SEM, and EDX. To select the best performing nanocomposite, screening studies were conducted for different GQD loadings and calcination temperatures. Physicochemical studies indicated that GQD−TiO_2 greatly improved the photocatalytic discoloration efficiency for RY145 dye. The best combination of GQD loading and calcination temperature was 15 and 300 °C, respectively, with RY145 discoloration of 99.3% in 30 min of visible light irradiation. Moreover, the photocatalytic reaction followed the PFO. In addition, the heterogeneous modeling (Langmuir−Hinshelwood isotherm) showed the dominant K_C value of 1.08 mg L^{-1} min^{-1} over the K_{LH} value (0.18 L mg^{-1}). The photocatalytic reaction mechanism studies were conducted to study the role of different active species and demonstrated that the superoxide ($O_2^{\bullet-}$) generated at the conduction band of the nanocomposite is the main active species in the GQD−TiO_2-

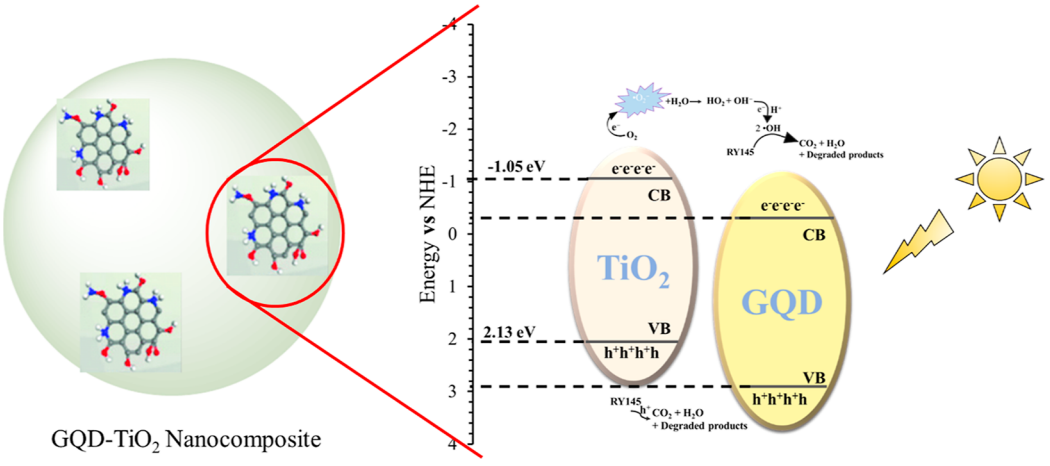

Figure 9. Proposed photocatalytic mechanism of 15GQD−TiO_2-300 for RY145 dye discoloration.

https://doi.org/10.1021/acsomega.2c05805
ACS Omega 2023, 8, 3007−3016

300. Additionally, the nanocomposite maintained its efficiency until the seventh cycle with a slight decline of 9% performance in the final cycle.

■ ASSOCIATED CONTENT

Supporting Information

The Supporting Information is available free of charge at https://pubs.acs.org/doi/10.1021/acsomega.2c05805.

Band gap estimation and UV−visible analysis of the synthesized GQDs and different reaction kinetic models including ZO, FO, and SO for the decolorization of RY145 using the 15GQD-TiO_2 nanocomposite (PDF)

■ AUTHOR INFORMATION

Corresponding Authors

Muhammad Saqib Khan − *Department of Environmental Sciences, COMSATS University Islamabad, 22020 Abbottabad, Pakistan;* Present Address: Faculty of Biomedical Sciences and Engineering, Department of Biomedical Sciences, Pak-Austria Fachhochschule: Institute of Applied Sciences and Technology, Mang, Haripur, KPK, Pakistan; orcid.org/0000-0002-0897-7436; Email: muhammadsaqib@yahoo.com

Ajmal Khan − *Natural and Medical Sciences Research Center, University of Nizwa, 616 Nizwa, Sultanate of Oman;* orcid.org/0000-0001-7851-6080; Email: ajmalkhan@unizwa.edu.om

Nadia Riaz − *Department of Environmental Sciences, COMSATS University Islamabad, 22020 Abbottabad, Pakistan;* orcid.org/0000-0002-0931-1089; Email: nadiariazz@gmail.com

Ahmed Al-Harrasi − *Natural and Medical Sciences Research Center, University of Nizwa, 616 Nizwa, Sultanate of Oman;* orcid.org/0000-0002-0815-5942; Email: aharrasi@unizwa.edu.om

Authors

Syeda Kinza Fatima − *Department of Environmental Sciences, COMSATS University Islamabad, 22020 Abbottabad, Pakistan*

Ansumana Sangi Ceesay − *Department of Environmental Sciences, COMSATS University Islamabad, 22020 Abbottabad, Pakistan; Department of Water Resources, Water Quality Laboratory, 00220 Banjul, The Gambia*

Rizwana Sarwar − *Department of Chemistry, COMSATS University Islamabad, 22020 Abbottabad, Pakistan*

Muhammad Bilal − *Department of Environmental Sciences, COMSATS University Islamabad, 22020 Abbottabad, Pakistan*

Jalal Uddin − *Department of Pharmaceutical Chemistry, College of Pharmacy, King Khalid University, 62529 Abha, Kingdom of Saudi Arabia*

Anwar Ul-Hamid − *Centre for Engineering Research, King Fahd University of Petroleum and Minerals, 31261 Dhahran, Saudi Arabia;* orcid.org/0000-0002-0259-301X

Complete contact information is available at: https://pubs.acs.org/10.1021/acsomega.2c05805

Funding

The project was supported by grant from The Oman Research Council (TRC) through the funded project (BFP/RGP/CBS/21/006).

Notes

The authors declare no competing financial interest.

■ ACKNOWLEDGMENTS

The authors extend their appreciation to the Deanship of Scientific Research at King Khalid University for funding this work through Small Groups under grant number (RGP.1/200/43). The authors would like to thank the University of Nizwa for the generous support. We thank the analytical and technical staff for their assistance.

■ REFERENCES

(1) Marimuthu, S.; Antonisamy, A. J.; Malayandi, S.; Rajendran, K.; Tsai, P.-C.; Pugazhendhi, A.; Ponnusamy, V. K. Silver nanoparticles in dye effluent treatment: A review on synthesis, treatment methods, mechanisms, photocatalytic degradation, toxic effects and mitigation of toxicity. *J. Photochem. Photobiol., B* **2020**, *205*, 111823.

(2) Berradi, M.; Hsissou, R.; Khudhair, M.; Assouag, M.; Cherkaoui, O.; El Bachiri, A.; El Harfi, A. Textile finishing dyes and their impact on aquatic environs. *Heliyon* **2019**, *5*, No. e02711.

(3) Yadav, A. K.; Jain, C.; Malik, D. Toxic characterization of textile dyes and effluents in relation to human health hazards. *J. Sustain. Environ. Res.* **2014**, *3*, 95−102.

(4) Ghodake, G. S.; Talke, A. A.; Jadhav, J. P.; Govindwar, S. P. POTENTIAL OFBRASSICA JUNCEAIN ORDER TO TREAT TEXTILE-EFFLUENT-CONTAMINATED SITES. *Int. J. Phytoremediation* **2009**, *11*, 297−312.

(5) Mahmood, Q.; Masood, F.; Bhatti, Z. A.; Siddique, M.; Bilal, M.; Yaqoob, H.; Farooq, R.; Ullah, Z. Biological treatment of the dye Reactive Blue 19 by cattails and anaerobic bacterial consortia. *Toxicol. Environ. Chem.* **2014**, *96*, 530−541.

(6) Shah, J. A.; Butt, T. A.; Mirza, C. R.; Shaikh, A. J.; Khan, M. S.; Arshad, M.; Riaz, N.; Haroon, H.; Gardazi, S. M. H.; Yaqoob, K.; Bilal, M. Phosphoric Acid Activated Carbon from Melia azedarach Waste Sawdust for Adsorptive Removal of Reactive Orange 16: Equilibrium Modelling and Thermodynamic Analysis. *Molecules* **2020**, *25*, 2118.

(7) Riaz, N.; Fen, D. A. C. S.; Khan, M. S.; Naz, S.; Sarwar, R.; Farooq, U.; Bustam, M. A.; Batiha, G. E.-S.; El Azab, I. H.; Uddin, J.; Khan, A. Iron-Zinc Co-Doped Titania Nanocomposite: Photocatalytic and Photobiocidal Potential in Combination with Molecular Docking Studies. *Catalysts* **2021**, *11*, 1112.

(8) Dalari, B. L. S. K.; Giroletti, C. L.; Malaret, F. J.; Skoronski, E.; Hallett, J. P.; Matias, W. G.; Puerari, R. C.; Nagel-Hassemer, M. E. Application of a phosphonium-based ionic liquid for reactive textile dye removal: Extraction study and toxicological evaluation. *J. Environ. Manage.* **2022**, *304*, 114322.

(9) Ihaddaden, S.; Aberkane, D.; Boukerroui, A.; Robert, D. Removal of methylene blue (basic dye) by coagulation-flocculation with biomaterials (bentonite and Opuntia ficus indica). *J. Water Proc. Eng.* **2022**, *49*, 102952.

(10) Yan, M.; Hua, Y.; Zhu, F.; Gu, W.; Jiang, J.; Shen, H.; Shi, W. Fabrication of nitrogen doped graphene quantum dots-BiOI/MnNb2O6 p-n junction photocatalysts with enhanced visible light efficiency in photocatalytic degradation of antibiotics. *Appl. Catal., B* **2017**, *202*, 518−527.

(11) Zhuo, S.; Shao, M.; Lee, S.-T. Upconversion and down-conversion fluorescent graphene quantum dots: ultrasonic preparation and photocatalysis. *ACS Nano* **2012**, *6*, 1059−1064.

(12) Riaz, N.; Kait, C. F.; Man, Z.; Dutta, B. K.; Ramli, R. M.; Khan, M. S. Visible Light Photodegradation of Azo Dye by Cu/TiO2. *Adv. Mater. Res.* **2014**, *917*, 151−159.

(13) Eslami, A.; Amini, M. M.; Yazdanbakhsh, A. R.; Mohseni-Bandpei, A.; Safari, A. A.; Asadi, A. N,S co-doped TiO2nanoparticles and nanosheets in simulated solar light for photocatalytic degradation of non-steroidal anti-inflammatory drugs in water: a comparative study. *J. Chem. Technol. Biotechnol.* **2016**, *91*, 2693−2704.

(14) Hajipour, P.; Eslami, A.; Bahrami, A.; Hosseini-Abari, A.; Saber, F. Y.; Mohammadi, R.; Yazdan Mehr, M. Surface modification of TiO2 nanoparticles with CuO for visible-light antibacterial applications and photocatalytic degradation of antibiotics. *Ceram. Int.* **2021**, *47*, 33875−33885.
(15) Fadaka, A.; Aluko, O.; Awawu, S.; Theledi, K. Green synthesis of gold nanoparticles using Pimenta dioica leaves aqueous extract and their application as photocatalyst, antioxidant, and antibacterial agents. *J. Multidiscip. Appl. Nat. Sci.* **2021**, *1*, 78.
(16) Ilhan, H.; Durmaz Cayci, G. B.; Aksoy, E.; Diker, H.; Varlikli, C. Photocatalytic activity of dye-sensitized and non-sensitized GO-TiO 2 nanocomposites under simulated and direct sunlight. *Int. J. Appl. Ceram. Technol.* **2022**, *19*, 425−435.
(17) Jeong, E.; Park, H. Y.; Lee, J.; Kim, H.-E.; Lee, C.; Kim, E.-J.; Hong, S. W. Long-term and stable antimicrobial properties of immobilized Ni/TiO2 nanocomposites against Escherichia coli, Legionella thermalis, and MS2 bacteriophage. *Environ. Res.* **2021**, *194*, 110657.
(18) Li, R.; Wang, D. Understanding the structure-performance relationship of active sites at atomic scale. *Nano Res.* **2022**, *15*, 6888−6923.
(19) Min, S.; Hou, J.; Lei, Y.; Ma, X.; Lu, G. Facile one-step hydrothermal synthesis toward strongly coupled TiO2/graphene quantum dots photocatalysts for efficient hydrogen evolution. *Appl. Surf. Sci.* **2017**, *396*, 1375−1382.
(20) Sudhagar, P.; Herraiz-Cardona, I.; Park, H.; Song, T.; Noh, S. H.; Gimenez, S.; Sero, I. M.; Fabregat-Santiago, F.; Bisquert, J.; Terashima, C.; Paik, U.; Kang, Y. S.; Fujishima, A.; Han, T. H. Exploring Graphene Quantum Dots/TiO2 interface in photoelectrochemical reactions: Solar to fuel conversion. *Electrochim. Acta* **2016**, *187*, 249−255.
(21) Chinnusamy, S.; Kaur, R.; Bokare, A.; Erogbogbo, F. Incorporation of graphene quantum dots to enhance photocatalytic properties of anatase TiO2. *MRS Commun.* **2018**, *8*, 137−144.
(22) Pan, D.; Jiao, J.; Li, Z.; Guo, Y.; Feng, C.; Liu, Y.; Wang, L.; Wu, M. Efficient Separation of Electron-Hole Pairs in Graphene Quantum Dots by TiO2 Heterojunctions for Dye Degradation. *ACS Sustainable Chem. Eng.* **2015**, *3*, 2405−2413.
(23) Long, R.; Casanova, D.; Fang, W.-H.; Prezhdo, O. V. Donor-Acceptor Interaction Determines the Mechanism of Photoinduced Electron Injection from Graphene Quantum Dots into TiO2: π-Stacking Supersedes Covalent Bonding. *J. Am. Chem. Soc.* **2017**, *139*, 2619−2629.
(24) Dong, Y.; Shao, J.; Chen, C.; Li, H.; Wang, R.; Chi, Y.; Lin, X.; Chen, G. Blue luminescent graphene quantum dots and graphene oxide prepared by tuning the carbonization degree of citric acid. *Carbon* **2012**, *50*, 4738−4743.
(25) Khan, M. S.; Riaz, N.; Shaikh, A. J.; Shah, J. A.; Hussain, J.; Irshad, M.; Awan, M. S.; Syed, A.; Kallerhoff, J.; Arshad, M.; Bilal, M. Graphene quantum dot and iron co-doped TiO2 photocatalysts: Synthesis, performance evaluation and phytotoxicity studies. *Ecotoxicol. Environ. Saf.* **2021**, *226*, 112855.
(26) Khan, M. S.; Shah, J. A.; Riaz, N.; Butt, T. A.; Khan, A. J.; Khalifa, W.; Gasmi, H. H.; Latifee, E. R.; Arshad, M.; Al-Naghi, A. A. A.; Ul-Hamid, A.; Arshad, M.; Bilal, M. Synthesis and Characterization of Fe-TiO2 Nanomaterial: Performance Evaluation for RB5 Decolorization and In Vitro Antibacterial Studies. *Nanomaterials* **2021**, *11*, 436.
(27) Iftikhar, A.; Khan, M. S.; Rashid, U.; Mahmood, Q.; Zafar, H.; Bilal, M.; Riaz, N. Influence of metallic species for efficient photocatalytic water disinfection: bactericidal mechanism of in vitro results using docking simulation. *Environ. Sci. Pollut. Res.* **2020**, *27*, 39819−39831.
(28) Houas, A.; Lachheb, H.; Ksibi, M.; Elaloui, E.; Guillard, C.; Herrmann, J.-M. Photocatalytic degradation pathway of methylene blue in water. *Appl. Catal., B* **2001**, *31*, 145−157.
(29) Wang, S. Q.; Liu, W. B.; Fu, P.; Cheng, W. L. Enhanced photoactivity of N-doped TiO2 for Cr(VI) removal: Influencing factors and mechanism. *Korean J. Chem. Eng.* **2017**, *34*, 1584−1590.
(30) Liao, L.-F.; Lien, C.-F.; Shieh, D.-L.; Chen, M.-T.; Lin, J.-L. FTIR Study of Adsorption and Photoassisted Oxygen Isotopic Exchange of Carbon Monoxide, Carbon Dioxide, Carbonate, and Formate on TiO2. *J. Phys. Chem. B* **2002**, *106*, 11240−11245.
(31) Teymourinia, H.; Salavati-Niasari, M.; Amiri, O.; Yazdian, F. Application of green synthesized TiO2/Sb2S3/GQDs nanocomposite as high efficient antibacterial agent against E. coli and Staphylococcus aureus. *Mater. Sci. Eng., C* **2019**, *99*, 296−303.
(32) Hao, X.; Jin, Z.; Xu, J.; Min, S.; Lu, G. Functionalization of TiO2 with graphene quantum dots for efficient photocatalytic hydrogen evolution. *Superlattices Microstruct.* **2016**, *94*, 237−244.
(33) Cheng, X.; Yu, X.; Xing, Z.; Yang, L. Synthesis and characterization of N-doped TiO2 and its enhanced visible-light photocatalytic activity. *Arab. J. Chem.* **2016**, *9*, S1706−S1711.
(34) Ziashahabi, A.; Prato, M.; Dang, Z.; Poursalehi, R.; Naseri, N. The effect of silver oxidation on the photocatalytic activity of Ag/ZnO hybrid plasmonic/metal-oxide nanostructures under visible light and in the dark. *Sci. Rep.* **2019**, *9*, 11839.
(35) Coleman, H.; Vimonses, V.; Leslie, G.; Amal, R. Degradation of 1,4-dioxane in water using TiO2 based photocatalytic and H2O2/UV processes. *J. Hazard. Mater.* **2007**, *146*, 496−501.
(36) Riaz, N.; Chong, F. K.; Dutta, B. K.; Man, Z. B.; Khan, M. S.; Nurlaela, E.Effect of calcination temperature on Orange II photocatalytic degradation using Cu:Ni/TiO_2 under visible light. *2011 National Postgraduate Conference*; IEEE. 19−20 Sept. 2011, 2011; pp 1−5.
(37) Shah, J. A.; Ashfaq, T.; Khan, M. S.; Riaz, N.; Shah, K. H.; Arshad, M.; Shah, S. H.; Amin, B. A. Z.; Arfan, M.; Zhang, Y.; Bilal, M. Melia azedarach Activated Carbon and its novel TiO_2 Nanocomposite for Chemisorption and Photodecoloration of Reactive Orange 16: Isotherm and Kinetic Modeling. *Curr. Anal. Chem.* **2020**, *17*, 107−119.
(38) Alkorbi, A. S.; Muhammad Asif Javed, H.; Hussain, S.; Latif, S.; Mahr, M. S.; Mustafa, M. S.; Alsaiari, R.; Alhemiary, N. A. Solar light-driven photocatalytic degradation of methyl blue by carbon-doped TiO2 nanoparticles. *Opt. Mater.* **2022**, *127*, 112259.
(39) Ghumro, S. S.; Lal, B.; Pirzada, T. Visible-Light-Driven Carbon-Doped TiO2-Based Nanocatalysts for Enhanced Activity toward Microbes and Removal of Dye. *ACS Omega* **2022**, *7*, 4333−4341.
(40) Aguedach, A.; Brosillon, S.; Morvan, J.; Lhadi, E. K. Photocatalytic degradation of azo-dyes reactive black 5 and reactive yellow 145 in water over a newly deposited titanium dioxide. *Appl. Catal., B* **2005**, *57*, 55−62.
(41) Nguyen, M. B.; Le, G. H.; Nguyen, T. D.; Nguyen, Q. K.; Pham, T. T. T.; Lee, T.; Vu, T. A. Bimetallic Ag-Zn-BTC/GO composite as highly efficient photocatalyst in the photocatalytic degradation of reactive yellow 145 dye in water. *J. Hazard. Mater.* **2021**, *420*, 126560.
(42) Khan, M. S.; Shah, J. A.; Arshad, M.; Halim, S. A.; Khan, A.; Shaikh, A. J.; Riaz, N.; Khan, A. J.; Arfan, M.; Shahid, M.; Pervez, A.; Al-Harrasi, A.; Bilal, M. Photocatalytic Decolorization and Biocidal Applications of Nonmetal Doped TiO2: Isotherm, Kinetic Modeling and In Silico Molecular Docking Studies. *Molecules* **2020**, *25*, 4468.
(43) Qiu, J.; Liu, F.; Yue, C.; Ling, C.; Li, A. A recyclable nanosheet of Mo/N-doped TiO2 nanorods decorated on carbon nanofibers for organic pollutants degradation under simulated sunlight irradiation. *Chemosphere* **2019**, *215*, 280−293.
(44) Paragas, L. K. B.; Dien Dang, R. S.; Sahu, S.; Garcia-Segura, M. D. G.; de Luna, J. A. I.; Pimentel, R.-A.; Doong, R.-A. Enhanced visible-light-driven photocatalytic degradation of acetaminophen over CeO2/I, K-codoped C3N4 heterojunction with tunable properties in simulated water matrix. *Sep. Purif. Technol.* **2021**, *272*, 117567.

https://doi.org/10.1021/acsomega.2c05805
ACS Omega 2023, 8, 3007−3016